



Pseudogap transition within the superconducting phase in the three-band Hubbard model

S. S. Dash  and D. Sénéchal *Département de physique and Institut quantique, Université de Sherbrooke, Sherbrooke, Québec, Canada J1K 2R1*

(Received 8 October 2019; revised manuscript received 20 November 2019; published 18 December 2019)

The onset of the pseudogap in high- T_c superconducting cuprates (HTSC) is marked by the T^* line in the doping-temperature phase diagram, which ends at a point p^* at zero temperature within the superconducting dome. Although various theoretical and experimental studies indicate a competition between the pseudogap and superconductivity, there is no general consensus on the effects of the pseudogap within the superconducting phase. We use cluster dynamical mean-field theory on a three-band Hubbard model for the HTSC to study the superconducting phase at $T = 0$, obtained when doping the charge-transfer insulator, for several values of U . We observe a first-order transition within the superconducting phase, which separates the underdoped and overdoped solutions. The transition to the underdoped solution is marked by a discontinuous increase in the spectral gap, and on further underdoping the spectral gap increases while the superconducting order parameter decreases. We conclude that this is due to the onset of the pseudogap in the underdoped region, which contributes to the increasing spectral gap; this is further consistent with the appearance of a pole in the normal component of the self-energy, in the antinodal region, in the underdoped solution. This is accompanied by a change in the source of the condensation energy from potential energy, in the overdoped region, to kinetic energy in the underdoped region. Further, we also observe that the d -wave node vanishes smoothly within the superconducting phase at low values of hole doping, within the underdoped region. We see this as a manifestation of Mott physics operating at very low doping. Various aspects of the results and their implications are discussed.

DOI: [10.1103/PhysRevB.100.214509](https://doi.org/10.1103/PhysRevB.100.214509)

I. INTRODUCTION

One of the most striking effects of strong correlations in hole-doped high- T_c superconducting cuprates (HTSC) is the pseudogap (PG). It manifests itself as a loss of density of states along the antinodal directions at temperatures less than T^* [1]. It has been considered a precursor of superconductivity, which would emerge on lowering the temperature further, below T_c [1–3]. However, such a picture has fallen out of favor since it has been observed that the T^* line ends within the superconducting dome at a doping p^* [4,5]. This means that the pseudogap and superconductivity have distinct origins.

Therefore, an important question to consider is whether the pseudogap coexists with d -wave superconductivity. Various studies have found evidence for the pseudogap within the superconducting (SC) phase [6–8]. Although the doping dependence is not very well understood, one view is that the magnitude of the gap does not vary much with doping, in the pseudogap phase below T_c [6,7,9]. On the other hand, Tanaka *et al.* [10] report that the antinodal gap, attributed to the pseudogap, increases with underdoping while the near-nodal gap, seen as a proxy to the SC gap, decreases. Kondo *et al.* [11] observe a similar competition between superconductivity and the pseudogap. Additionally, there is evidence of a nodeless SC gap at very low values of hole doping [7,12]; whether it is related to the pseudogap is not clear. On the theoretical side, there have been studies indicating strong signatures of a quantum critical point within the SC state associated with strong momentum-space differentiation [13,14]. In particular, Civelli *et al.* [15] suggest two gap energy scales within the SC phase. These studies point to an inherent competition between the pseudogap and superconducting phases.

The relevant physics of HTSC lies mostly in the copper oxide planes. It has long been thought that the one-band Hubbard model should capture the basic physics of cuprates (d -wave superconductivity and the pseudogap), but it is only since the advent of sophisticated numerical methods that this could be confirmed [16–19]. A review on the origin of the pairing interaction in the Hubbard model is given in Ref. [20]. Cluster extensions of DMFT have been particularly successful in capturing the strong correlation physics in cuprates [16,17]. These methods take into account the short-range correlations, which are crucial for d -wave superconductivity [21]. However, the one-band model fails to capture the dynamics of holes in cuprates, which mostly reside on the oxygen orbitals [22]. A more accurate model is a three-band Hubbard model [23–25], which involves the copper $3d_{x^2-y^2}$ orbital and the two oxygen $2p$ orbitals in each CuO_2 unit cell. A recent work by Fratino *et al.* [26] using the three-band Hubbard model shows that holes are indeed located in the oxygen orbitals upon doping.

In this work, we study the SC state appearing when doping the charge-transfer insulator within the three-band Hubbard model, using cluster dynamical mean-field theory (CDMFT) with an exact diagonalization impurity solver at zero temperature. We observe three SC regimes in our computations: (i) at large hole doping, BCS-like superconductivity with a symmetric gap in the density of states (DOS); (ii) at moderate hole doping, superconductivity coexists with the pseudogap, and the DOS displays a large, asymmetric gap; this is separated from the first regime by a first-order transition; (iii) at low doping, superconductivity becomes fully gapped. Although our observations seem to be in line with the zero-temperature

scenario of the trisected SC dome with three distinct phases proposed by Vishik *et al.* [7], we observe signatures of only one discontinuous transition, corresponding to the onset of the pseudogap, i.e., between (i) and (ii). We ignore the possibility of magnetic phases, in particular antiferromagnetism, in order to keep the computations simple.

The paper is organized as follows. In Sec. II, we present the model and briefly describe the method used. In Sec. III, we show our results and propose possible interpretations. Broader implications of our results are discussed in Sec. IV.

II. MODEL AND METHOD

A. Three-band Hubbard model

We use a modified three-band Emery model [25] to describe the CuO₂ planes, consisting of a Cu $3d_{x^2-y^2}$ orbital

$$H_0(\mathbf{k}) = \begin{pmatrix} \epsilon_d - \mu & t_{pd}(1 - e^{-ik_x}) & t_{pd}(1 - e^{-ik_y}) \\ t_{pd}(1 - e^{ik_x}) & \epsilon_p - \mu + 2t_{pp'} \cos k_x & t_{pp}(1 - e^{ik_x})(1 - e^{-ik_y}) \\ t_{pd}(1 - e^{ik_y}) & t_{pp}(1 - e^{-ik_x})(1 - e^{ik_y}) & \epsilon_p - \mu + 2t_{pp'} \cos k_y \end{pmatrix}. \quad (2)$$

ϵ_d and ϵ_p are the orbital energies of the $3d$ and $2p$ orbitals, respectively. μ is the chemical potential. t_{pd} is the absolute value of the first neighbor hopping integral between $3d$ and $2p$ orbitals (brown bonds in Fig. 1), t_{pp} is the absolute value of the first neighbor hopping integral between two $2p$ orbitals (green bonds in Fig. 1), and $t_{pp'}$ is the absolute value of the hopping integral between two $2p$ orbitals separated by a Cu atom (orange bonds in Fig. 1). Note that the Cu orbitals are not directly connected.

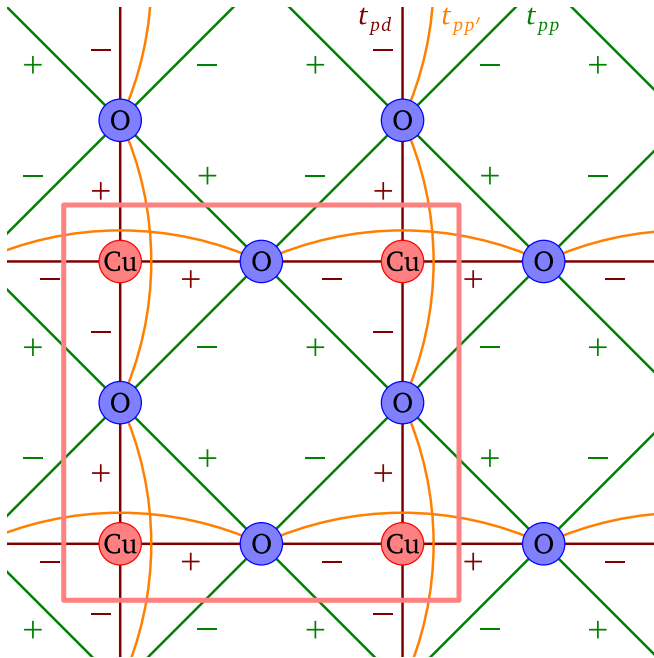


FIG. 1. Sketch of the CuO₂ lattice. The signs on the hopping terms in (2) are indicated and are the result of the combined phase of the orbitals participating in bonding. The four-site cluster of copper atoms used in CDMFT is indicated (red box).

and two O $2p$ orbitals within a unit cell. The Hamiltonian is expressed as

$$H = H_0 + U_d \sum_i n_{i\uparrow}^{(d)} n_{i\downarrow}^{(d)}. \quad (1)$$

H_0 is the noninteracting Hamiltonian. U_d is the on-site Coulomb repulsion on the Cu $3d_{x^2-y^2}$ orbitals. $n_{i\sigma}^{(d)}$ is the number operator for electrons with spin- σ at the copper site i . The Coulomb repulsion U_p on the O $2p$ orbitals is neglected.

The noninteracting Hamiltonian H_0 is often expressed as a hopping matrix in \mathbf{k} space:

We use two sets of parameters in this work. One is taken from Fratino *et al.* [26] and provides a simple scenario for obtaining a charge-transfer gap [27]:

$$t_{pp} = 1, \quad t_{pp'} = 1, \quad t_{pd} = 1.5, \quad \epsilon_d = 0, \quad \epsilon_p = 7. \quad (3)$$

The second is more realistic, corresponds to Bi-2212, and is obtained from *ab initio* calculations by Weber *et al.* [28]:

$$t_{pp} = 1, \quad t_{pp'} = 0.2, \quad t_{pd} = 2.1, \quad \epsilon_d = 0, \quad \epsilon_p = 2.5. \quad (4)$$

B. Cluster dynamical mean-field theory

In cluster dynamical mean-field theory, the infinite lattice is tiled into identical clusters, and each cluster's lattice environment is replaced by a set of uncorrelated orbitals (the “bath”). This cluster-bath system defines an Anderson-impurity model, which must be solved for the Green function $\mathbf{G}_c(\omega)$ using an *impurity solver*. In this work, we use an exact diagonalization solver at $T = 0$ and therefore are limited to a small number of bath orbitals. The cluster self-energy $\mathbf{\Sigma}(\omega)$ is then extracted using Dyson's equation

$$\mathbf{G}_c(\omega)^{-1} = \omega - \mathbf{t}_c - \mathbf{\Gamma}(\omega) - \mathbf{\Sigma}(\omega), \quad (5)$$

where \mathbf{t}_c is the hopping matrix on the cluster and $\mathbf{\Gamma}(\omega)$ the *hybridization function*, which depends on the bath parameters, i.e., the energies of the uncorrelated orbitals and their hybridization with the cluster. Note that here we have used the symbol $\mathbf{\Gamma}$ for the hybridization function, instead of $\mathbf{\Delta}$ which is generally used in the context of DMFT. The cluster self-energy is then used as an approximation to be the full lattice self-energy, so that the lattice Green function $\mathbf{G}(\tilde{\mathbf{k}}, \omega)$ is expressed as

$$\mathbf{G}(\tilde{\mathbf{k}}, \omega)^{-1} = \omega - \mathbf{t}(\tilde{\mathbf{k}}) - \mathbf{\Sigma}(\omega), \quad (6)$$

where $\tilde{\mathbf{k}}$, the *reduced* wave vector, belongs to the Brillouin zone of the superlattice and $\mathbf{t}(\tilde{\mathbf{k}})$ is the one-body matrix of the

model, expressed in a mixed basis of cluster sites and reduced wave vector $\tilde{\mathbf{k}}$. The bath parameters are chosen in such a way as to minimize the difference between $\mathbf{G}_c(\omega)$ and the Fourier transform of $\mathbf{G}(\tilde{\mathbf{k}}, \omega)$, i.e., its local version. Details can be found in Refs. [17,29–31].

In this work, the impurity cluster (red box in Fig. 1) contains 4 Cu atoms which are connected to the bath. As far as the CDMFT procedure is concerned, only the copper part of the lattice Green function $\mathbf{G}_{\text{Cu}}(\tilde{\mathbf{k}}, \omega)$ is taken into account:

$$\mathbf{G}_{\text{Cu}}(\tilde{\mathbf{k}}, \omega)^{-1} = \omega - \mathbf{t}_{\text{Cu}}(\tilde{\mathbf{k}}) - \mathbf{\Gamma}_O(\tilde{\mathbf{k}}, \omega) - \mathbf{\Sigma}(\omega), \quad (7)$$

which contains a fixed hybridization function $\mathbf{\Gamma}_O(\tilde{\mathbf{k}}, \omega)$ coming from the oxygen orbitals. Since the oxygen orbitals are uncorrelated in our model, their effect can be exactly represented by the hybridization function $\mathbf{\Gamma}_O(\tilde{\mathbf{k}}, \omega)$ [26]. The presence of $\mathbf{\Gamma}_O(\tilde{\mathbf{k}}, \omega)$ in the lattice Green function ensures that the effect of the oxygen orbitals is included in the self-energy through the CDMFT self-consistency procedure.

In this work, the cluster-bath system contains four copper sites and eight bath orbitals. In order to probe superconductivity, we include anomalous hybridizations between bath and cluster, along with regular hybridizations. The Nambu formalism is used in order to incorporate both the normal and anomalous components of the Green function into a single object. The bath parametrization is based on the irreducible representations of the point group C_{2v} [32,33]. In this bath parametrization, the bath Hamiltonian is diagonal and each bath orbital is connected to all cluster sites. Details of the bath parametrization using the point group C_{2v} can be found in Foley *et al.* [32].

The average value of an one-body operator $\hat{O} = \sum_{\alpha,\beta} O_{\alpha\beta} d_{\alpha}^{\dagger} d_{\beta}$, where $d_{i\sigma}$ annihilates an electron of spin σ on Copper site i , is obtained from the lattice Green function (7) as

$$\langle \hat{O} \rangle = \oint \frac{d\omega}{2\pi} \int \frac{d^2\tilde{\mathbf{k}}}{(2\pi)^2} \text{tr}[\mathbf{O}(\tilde{\mathbf{k}})\mathbf{G}_{\text{Cu}}(\tilde{\mathbf{k}}, \omega)], \quad (8)$$

where $\tilde{\mathbf{k}}$ is a reciprocal lattice vector of the superlattice.

III. RESULTS

At a filling of five electrons per unit cell, the system is a charge-transfer insulator (CTI). This is different from a Mott insulator in the sense that the insulating gap is not between the two Hubbard bands but between the oxygen band and the upper Hubbard band. On doping with holes, these primarily go into the O $2p$ orbitals, as observed in experiments [22]. This is consistent with our observations and is evident from the cartoon in Fig. 2. Within our model, this is because the orbital energy of the O $2p$ orbitals is higher than that of the Cu $3d_{x^2-y^2}$ orbitals, making it expensive for electrons to reside in the oxygen orbitals.

Doping the CTI makes it susceptible to d -wave superconductivity [34]. Figure 3 shows the d -wave order parameter computed from the lattice Green function obtained from the converged CDMFT solutions, as a function of hole doping, for several values of U_d , all beyond the critical value U_d^c , that is, beyond the metal-insulator transition point. The order parameter is defined as $\psi = \langle \hat{\Delta} \rangle / N_s$, where N_s is the number

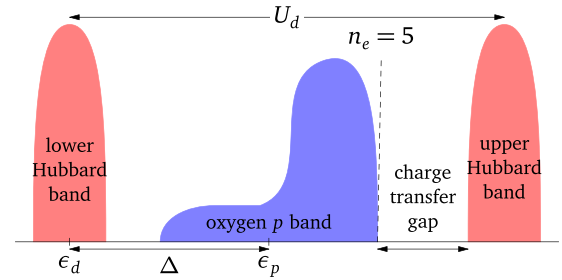


FIG. 2. Cartoon of the density of states (DOS) of the three-band Hubbard model. U_d splits the Copper band (red) into two subbands; the system is insulating at a filling of five electrons per unit cell when U_d is large enough to push the upper subband beyond the oxygen band. Because electrons migrate from the Cu $3d$ orbitals to the O $2p$ as U_d is increased, the insulator formed is called a charge-transfer insulator (CTI) and the associated gap is called the charge-transfer gap.

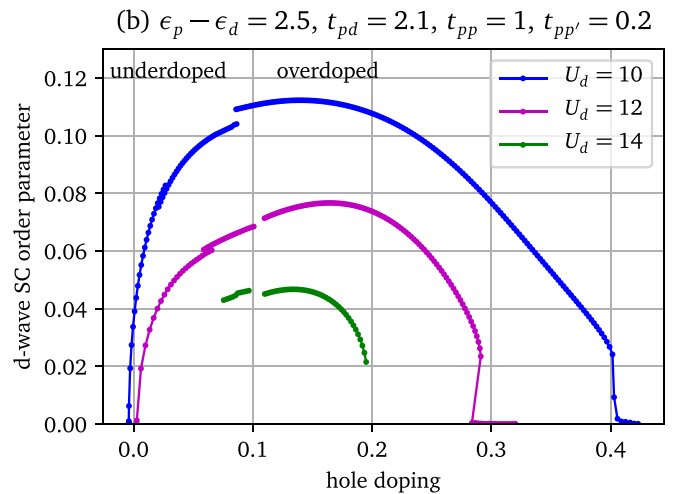
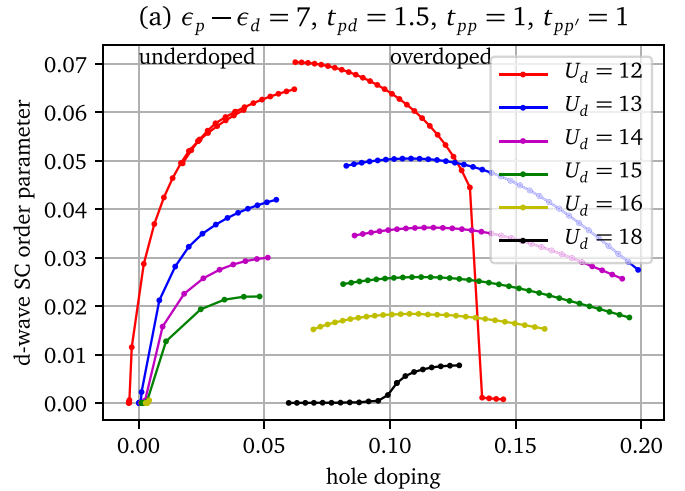


FIG. 3. d -wave order parameter vs doping at different values of U_d , higher than the critical value for the metal-insulator transition at a filling of five electrons in the unit cell, for (a) parameters (3) and (b) parameters (4). The critical value of U_d is around 11.7 for parameters (3) and around 9.2 for parameters (4).

of sites in the lattice and

$$\hat{\Delta} = \sum_{\langle ij \rangle_x} (d_{i,\uparrow} d_{j,\downarrow} - d_{i,\downarrow} d_{j,\uparrow}) - \sum_{\langle ij \rangle_y} (d_{i,\uparrow} d_{j,\downarrow} - d_{i,\downarrow} d_{j,\uparrow}) + \text{H.c.}, \quad (9)$$

where $\langle ij \rangle_x$ indicates a sum over nearest-neighbor copper sites in the x direction, and likewise for the y direction. In practice, it is computed from the anomalous part of the Green function (the Gor'kov function).

For all values of U_d , except $U_d = 18$ with parameters (3), the order parameter reveals the existence of two solutions, which we label “underdoped” and “overdoped.” In particular, a hysteresis in the value of the order parameter is observed for $U_d = 12$ and parameters (3) [Fig. 3(a)], as well as for $U_d = 10$ and parameters (4) [Fig. 3(b)]. This indicates a first-order transition between the two solutions. For higher values of U_d [$U_d > 12$ for parameters (3) and $U_d > 10$ for parameters (4)], there is a range of chemical potential μ between the overdoped and underdoped solutions in which the CDMFT procedure does not converge, which indicates a fundamentally unstable region that cannot be probed with our discrete bath framework. We assume this to be fundamentally similar to the first-order transitions seen at lower values of U_d , since both situations share the same physics across the discontinuity as we discuss later. The on-site Coulomb interaction U_d tends to suppress the order parameter. Furthermore, the underdoped solution with parameters (3) has disappeared at $U_d = 18$ [Fig. 3(a)].

The slightly negative hole doping seen in Fig. 3 is due to our use of the lattice average of electron density, as per Eq. (8), instead of the average computed from the impurity model ground state. The latter cannot be used since the oxygen orbitals are not contained in the impurity model.

Let us note that our system is in no way biased towards d -wave superconductivity except for the fact that the bath parametrization is based on the irreducible representations of the point group C_{2v} , which is compatible with the d -wave symmetry. In principle, we could also find extended s -wave superconductivity, which is also compatible with the C_{2v} point group, but the corresponding order parameter vanishes in our solutions.

The onset of superconductivity opens up a d -wave gap in the spectrum [35,36], which results in a partial gapping out of the DOS at low energy. We can get some insight into the nature of the underdoped and overdoped solutions by looking at the DOS close to the Fermi energy (Fig. 4). The superconducting (SC) gap, both in the underdoped and overdoped CDMFT solutions, is compared to the SC gap within a mean-field model with Hamiltonian $H_{\text{MF}} = H_0 + \Delta \hat{\Delta}$. The d -wave mean-field Δ and the chemical potential in H_0 are adjusted so that the order parameter and the electron density match the corresponding CDMFT solution.

The mean-field DOS obtained from H_{MF} (red curves in Fig. 4) contains the pure d -wave gap, in contrast with the SC gap arising from strong correlation effects in our CDMFT solutions (blue curves). In the overdoped solution [Fig. 4(a)], the SC gap is qualitatively similar in shape to that of the pure d -wave mean-field SC gap. However, in the underdoped

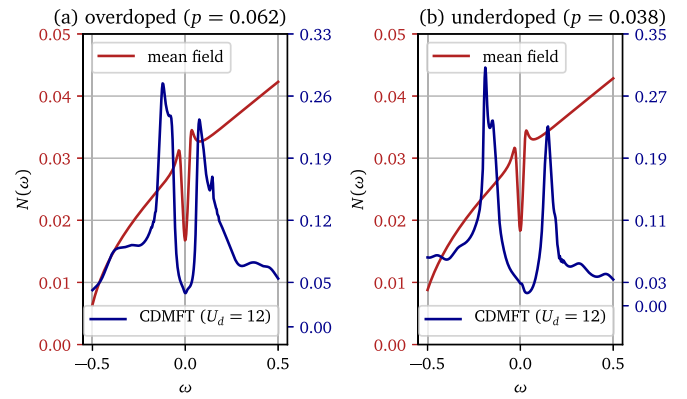


FIG. 4. DOS of the CDMFT solution for parameters (3) at $U_d = 12$ (in blue) compared with the mean-field DOS (in red), for both (a) overdoped and (b) underdoped solutions. The parameters of the mean-field Hamiltonian are adjusted to yield the same order parameter and density as those of the corresponding CDMFT solution. Note that the background of the gap in the CDMFT solutions is entirely different than that in the mean-field solutions, indicating a nontrivial redistribution of quasiparticle weight compared to the uncorrelated dispersion.

solution [Fig. 4(b)], the gap is strikingly different from the corresponding mean-field gap as well as from the gap in the overdoped solution: it is asymmetric and noticeably wider. This reveals the nontrivial effects of strong correlations in the underdoped solution. Hence there is a fundamental difference in the nature of the underdoped and overdoped solutions.

In order to understand the origin of the large gap in the underdoped solution and its relation with superconductivity, we show a plot of the magnitude of the gap in the DOS, along with the SC order parameter, as a function of hole doping (Fig. 5). In the overdoped solution, the spectral gap and the SC order parameter both increase towards zero doping. This indicates that the primary source of the gap in this solution

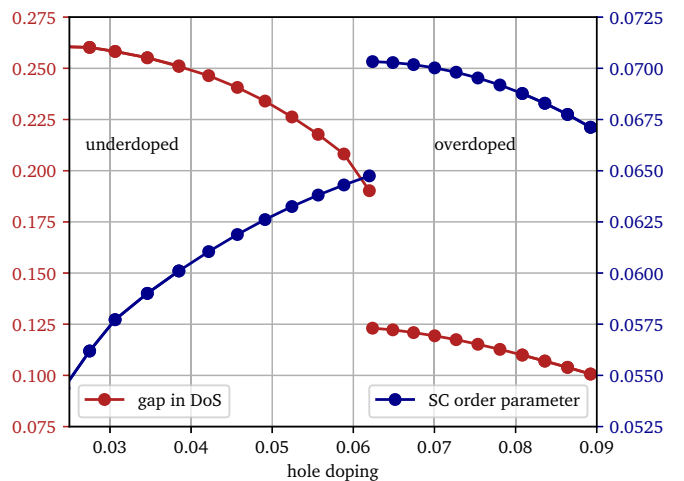


FIG. 5. Momentum-integrated spectral gap (red curve) and d -wave order parameter (blue curve) within the SC state, as a function of hole doping, for parameters (3) and $U_d = 12$. The gap in the DOS $N(\omega)$ is calculated as the distance between the two points above and below the Fermi level where $d^2N(\omega)/d\omega^2 = 0$.

is d -wave superconductivity, although correlations make it wider than the mean-field gap [Fig. 4(a)]. In contrast, the gap in the underdoped solution increases while the order parameter decreases [17]. Hence it is evident that the dominant source of the gap in the underdoped solution is not d -wave superconductivity but something else.

Let us place our observations in the context of the phenomenology of cuprates. The onset of the pseudogap in hole-doped cuprates is marked by the T^* line [37]. It was long thought that the SC gap might emerge from the normal state pseudogap [38]. However, it has been shown that, in the normal state, the T^* line ends within the SC dome at a point called p^* [4,5,39], indicating that superconductivity and the pseudogap are not directly related. Within this context, the first-order transition between the overdoped and underdoped solutions could be understood in terms of a pseudogap transition. This could explain the increase of the gap magnitude even when the order parameter is decreasing in the underdoped solution (Fig. 5), and also the large asymmetric gap [Fig. 4(b)]. Within the normal state, the onset of the pseudogap leads to the destruction of the Fermi surface into Fermi arcs, essentially partially gapping the Fermi surface [1] starting from the antinodal region in the Brillouin zone. Within a SC state, where we already have a d -wave gap [37,40], it is difficult to find a signature of the onset of the pseudogap in $A(\mathbf{k}, 0)$. Hence, as discussed earlier, we look at the momentum-integrated gap to find the signature of the pseudogap.

The pseudogap is a normal state property, and we indeed see its signatures in the normal state CDMFT solutions as well, namely the appearance of Fermi arcs, for $U_d = 12$ and parameters (3) (not shown). The normal state CDMFT solutions, obtained with ED as the impurity solver, have a limitation that there is a first-order transition corresponding to a particle number change in the impurity model. Therefore, although we see a first-order transition corresponding to the onset of the pseudogap in the normal state, we cannot definitely connect it to the first-order transition in the SC state, since the transition in our normal state is also accompanied by a particle number change in the impurity model.

Hence we instead look at the normal component of the cluster self-energy at the antinode (Fig. 6) to look for a signature of the pseudogap. The first order transition seen in Fig. 3 occurs between the red and green curves in Fig. 6 (they have the same doping value because of a hysteresis between the overdoped and underdoped solutions). The green curve, which belongs to the underdoped solution, displays a peak (marked by the green dotted line), absent from the overdoped solution (red and maroon curves). This peak grows with underdoping and leads to the insulating gap at zero doping (light blue curve). The pseudogap is generated by such a pole close to the Fermi level as discussed in Refs. [41–43]. This is also consistent with the fact that the pseudogap originates from Mott physics [44,45], and hence strengthens our interpretation of the underdoped solution as the pseudogap state.

It is known that the nature of superconductivity changes from being driven by potential energy in the weakly interacting limit to being driven by kinetic energy in the strong interaction limit. Previous studies have reported this crossover as a function of interaction across the Mott transition [46], as well as of hole doping [47] across the finite-doping Mott

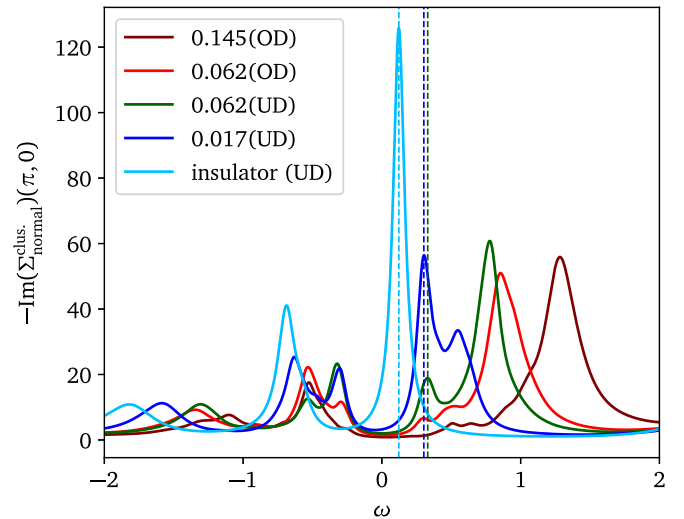


FIG. 6. Imaginary part of the normal component of the cluster self-energy is shown at the antinodal momentum [$\mathbf{k} = (\pi, 0)$] as a function of frequency ω , for several values of doping. Parameters (3) are used and $U_d = 12$. The underdoped curves (marked as UD) show a peak corresponding to the pole in the self-energy close to the Fermi level (marked by dotted lines), which is absent from the overdoped curves (marked as OD).

transition [48]. Figure 7 shows the potential and kinetic energy gains in our CDMFT SC solutions (relative to the normal state CDMFT solutions) as a function of doping. It shows that

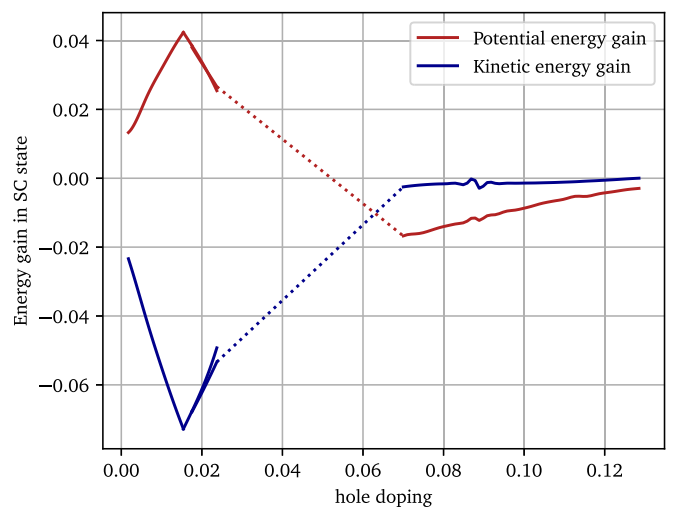


FIG. 7. Differences in kinetic and potential energies between the superconducting state and the normal state as a function of doping for parameters (3) and $U_d = 12$. Superconductivity in underdoped and overdoped solutions is driven by kinetic energy and potential energy, respectively. The normal state CDMFT solution is obtained with conserved particle number and spin, as opposed to the superconducting state which is obtained with conserved spin only. The normal state sees a transition corresponding to a particle number change accompanied by a jump in hole doping; hence we do not have the normal state solutions for a range of hole doping. We use a linear interpolation of the energy differences in that region, shown here by dotted lines.

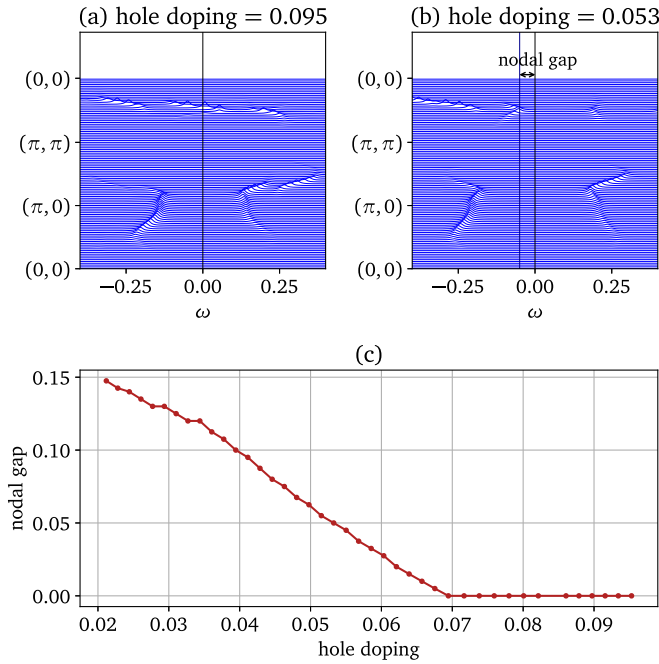


FIG. 8. Spectral function $A(\mathbf{k}, \omega)$ along the path $(0, 0) \rightarrow (\pi, 0) \rightarrow (\pi, \pi) \rightarrow (0, 0)$ in the Brillouin zone at $U_d = 10$, for the SC state with parameters (4) (a) with node and (b) without node. (c) Gap at the node as a function of hole doping. The spectral function is obtained from the periodized Green function [49]. The nodal gap is measured from the Fermi level to the point below it where the slope of $A(\mathbf{k}, \omega)$ first vanishes, i.e., at a peak.

superconductivity is stabilized mostly by potential energy in the overdoped region, as in BCS, and by kinetic energy in the underdoped region. This indicates the effect of strong correlation physics in the underdoped solution and is consistent with the interpretation of the underdoped solution as the pseudogap state [44,48].

Additionally, we observe a second, small hysteresis in the underdoped solutions for $U_d = 12$ and parameters (3) as well as for $U_d = 10, 12$ and parameters (4) (Fig. 3). We do not see any qualitative physical consequences of this, except for a small readjustment of the average values; we assume this to be just an effect of the discrete bath and hence consider it to be unphysical. The effect of this small hysteresis can also be seen in the condensation energy (Fig. 7) at 2% doping, but it does not change the physics of the solutions, i.e., the source of the condensation energy. This reinforces the fact that such an effect can be considered as an unphysical artifact of the method.

Another interesting feature of our results is the gradual disappearance of the nodes in the zero-frequency spectral function $A(\mathbf{k}, 0)$ along the diagonal direction. These nodes, a hallmark of d -wave superconductivity, disappear at a doping lower than the pseudogap transition (Fig. 8), while the SC order parameter is still finite, leading to an unusual scenario of nodeless d -wave superconductivity. In this regime, the low-energy DOS develops a full gap (not shown), which we understand as an effect of strong correlations gapping the quasiparticles within the SC state. It occurs at a doping higher than the unphysical hysteresis in Fig. 3; hence we think it is

not related to that. Such a nodeless superconducting regime has also been observed with ARPES [7], where it is identified as a distinct phase. However, we do not observe any signs of a sharp transition leading to this nodeless superconductivity: no new long-range order appears across this transition. Rather, it appears as a continuous change.

IV. DISCUSSION AND CONCLUSION

Theoretical studies using the one-band Hubbard model have observed a crossover between the overdoped and underdoped solutions identified with different doping dependencies of the nodal and antinodal gaps [14,15]. In our calculations with the three-band Hubbard model, we observe a first-order transition clearly marking the transition from the overdoped solution, in which the d -wave order parameter increases with the gap in the DOS, to the underdoped solution in which the d -wave order parameter decreases as the DOS gap increases. The onset of such a large, increasing gap, after the transition, on the underdoped side further indicates that this corresponds to the pseudogap (PG) transition. This is further accompanied by the appearance of a pole in the normal self-energy at the antinodal region, which is known to generate the pseudogap [41,42]. Thus the three-band model captures a richer correlation physics than the one-band model.

The experimental doping value at which the PG ends at zero temperature, $p^* \approx 0.2$, is much higher than the doping at which we observe the PG transition. It is even off by around 0.1 for parameters (4) which correspond to Bi-2212. In experiments, the doping values are mostly determined using the universal relation $T_c/T_c^{\max} = 1 - 82.6(p - 0.16)^2$, which is verified to hold for most of the cuprate families [50]. The origin of the mismatch between the experimental p^* and the value we observe in our computations is not clear. For example, the exact value of the band parameters can depend on the particular downfolding method used from the *ab initio* band structure. It may also be that the value of p^* is affected by the suppression of superconductivity in the experiments.

Also, the optimal doping observed in experiments is lower than the p^* point [7,51]. Optimal doping is defined in terms of the maximum SC critical temperature T_c . At doping lower than the PG transition, the SC order parameter decreases in our CDMFT solutions. This is in an apparent contradiction with experiments if we assume that T_c somehow indicates the strength of the order parameter. However, there seems to be no monotonic relation between T_c and the order parameter [26,47].

The PG transition appears as a first-order transition in the SC state at zero temperature. We observe the transition as a jump in the value of the order parameter across a region of hole doping (represented schematically by the gray regions in Fig. 9). An important question is the fate of this transition at finite temperature. Our first assumption is that the transition would follow the T^* line since we associate it with the onset of the PG. We can expect the transition to end at a critical point (say T_p), above which it exists as a crossover. There are three possible scenarios regarding where T_p lies: (a) below T_c [Fig. 9(a)], (b) above T_c [Fig. 9(b)], or (c) exactly at T_c [Fig. 9(c)]. In the finite-temperature CDMFT study of the three-band model by Fratino *et al.* [26] with continuous-time

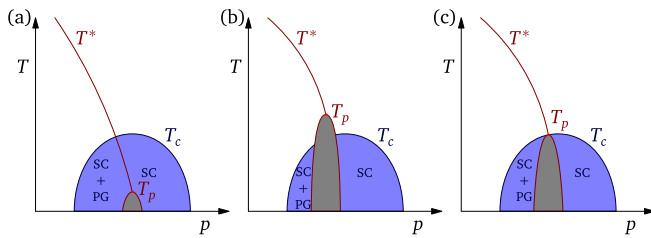


FIG. 9. Three scenarios are possible for the finite temperature behavior of the pseudogap (PG) transition depending upon the value of the PG critical point T_p relative to the superconducting (SC) critical temperature T_c : (a) $T_p < T_c$; (b) $T_p > T_c$; (c) $T_p = T_c$

quantum Monte Carlo (CTQMC) as the impurity solver, no transition is seen within the SC phase. Since low temperatures are difficult to reach in CTQMC, it might be that T_p lies below the lowest temperature they could probe. It could also be that their resolution in doping is too low to observe the transition, even if T_p were higher. Moreover, they observe the finite-doping Mott transition [48] in the normal state, whose high-temperature precursor is the T^* line. It seems reasonable that the first-order transition we observe is a manifestation of the finite-doping Mott transition, within the SC phase.

One limitation of the present study is the small size of our impurity model (four cluster sites and eight bath sites). The spatial fluctuations in our calculations are restricted by the four cluster sites. And typically two bath sites per correlated site is considered [52] to adequately capture the dynamical fluctuations; hence the size of the bath depends on the size

of the cluster. It is possible that increasing the size of the impurity model, which is very difficult to do at the moment at zero temperature, could decrease the range of the first-order transition; it could eventually become second order, i.e., a quantum critical point, in the thermodynamic limit. However, a recent slave-boson calculation with the t - J model also shows indication of a first-order pseudogap transition [53].

To summarize, we applied cluster dynamical mean-field theory to the three-band Hubbard model for the cuprates at zero temperature. We found two distinct superconducting solutions, separated by a first-order transition as a function of hole doping. We interpret the underdoped solution as a manifestation of the pseudogap below T_c , as shown by an associated jump in the spectral gap, along with the appearance of a pole in the antinodal self-energy, and a change in the nature of the condensation energy (potential vs kinetic). In addition, within the underdoped solution, the d -wave nodes smoothly disappear very close to the insulating state. These results are compatible with the sharp changes in the spectral gap observed as a function of doping in ARPES [7,10].

ACKNOWLEDGMENTS

Fruitful discussions with S. Verret, A.-M. Tremblay, A. Foley, S. Sakai, A. Mallik, S. Chen, and G. Sordi are gratefully acknowledged. Computational resources for this work were provided by Compute Canada and Calcul Québec. This work has been supported by the Natural Sciences and Engineering Research Council of Canada (NSERC) under Grant No. RGPIN-2015-05598.

- [1] T. Timusk and B. Statt, The pseudogap in high-temperature superconductors: An experimental survey, *Rep. Prog. Phys.* **62**, 61 (1999).
- [2] V. J. Emery and S. A. Kivelson, Importance of phase fluctuations in superconductors with small superfluid density, *Nature (London)* **374**, 434 (1995).
- [3] Ch. Renner, B. Revaz, J.-Y. Genoud, K. Kadowaki, and Ø. Fischer, Pseudogap Precursor of the Superconducting Gap in Under- and Overdoped $\text{Bi}_2\text{Sr}_2\text{CaCu}_2\text{O}_{8+\delta}$, *Phys. Rev. Lett.* **80**, 149 (1998).
- [4] J. L. Tallon and J. W. Loram, The doping dependence of T^* —what is the real High- T_c phase diagram? *Physica C: Superconductivity* **349**, 53 (2001).
- [5] R. Daou, N. Doiron-Leyraud, D. LeBoeuf, S. Y. Li, F. Laliberté, O. Cyr-Choiniere, Y. J. Jo, L. Balicas, J.-Q. Yan, J.-S. Zhou *et al.*, Linear temperature dependence of resistivity and change in the fermi surface at the pseudogap critical point of a high- T_c superconductor, *Nat. Phys.* **5**, 31 (2009).
- [6] K. McElroy, D.-H. Lee, J. E. Hoffman, K. M. Lang, J. Lee, E. W. Hudson, H. Eisaki, S. Uchida, and J. C. Davis, Coincidence of Checkerboard Charge Order and Antinodal State Decoherence in Strongly Underdoped Superconducting $\text{Bi}_2\text{Sr}_2\text{CaCu}_2\text{O}_{8+\delta}$, *Phys. Rev. Lett.* **94**, 197005 (2005).
- [7] I. M. Vishik, M. Hashimoto, R.-H. He, W.-S. Lee, F. Schmitt, D. Lu, R. G. Moore, C. Zhang, W. Meevasana, T. Sasagawa *et al.*, Phase competition in trisected superconducting dome, *Proc. Natl. Acad. Sci. USA* **109**, 18332 (2012).
- [8] B. Loret, S. Sakai, S. Benhabib, Y. Gallais, M. Cazayous, M. A. Méasson, R. D. Zhong, J. Schneeloch, G. D. Gu, A. Forget *et al.*, Vertical temperature boundary of the pseudogap under the superconducting dome in the phase diagram of $\text{Bi}_2\text{Sr}_2\text{CaCu}_2\text{O}_{8+\delta}$, *Phys. Rev. B* **96**, 094525 (2017).
- [9] M. Hashimoto, I. M. Vishik, R.-H. He, T. P. Devereaux, and Z.-X. Shen, Energy gaps in high-transition-temperature cuprate superconductors, *Nat. Phys.* **10**, 483 (2014).
- [10] K. Tanaka, W. S. Lee, D. H. Lu, A. Fujimori, T. Fujii, I. Terasaki, D. J. Scalapino, T. P. Devereaux, Z. Hussain, Z.-X. Shen *et al.*, Distinct fermi-momentum-dependent energy gaps in deeply underdoped $\text{Bi}2212$, *Science* **314**, 1910 (2006).
- [11] T. Kondo, R. Khasanov, T. Takeuchi, J. Schmalian, and A. Kaminski, Competition between the pseudogap and superconductivity in the high- T_c copper oxides, *Nature (London)* **457**, 296 (2009).
- [12] E. Razzoli, G. Drachuck, A. Keren, M. Radovic, N. C. Plumb, J. Chang, Y.-B. Huang, H. Ding, J. Mesot, and M. Shi, Evolution from a Nodeless Gap to $d_{x^2-y^2}$ -Wave in Underdoped $\text{La}_{2-x}\text{Sr}_x\text{CuO}_4$, *Phys. Rev. Lett.* **110**, 047004 (2013).
- [13] K. Haule and G. Kotliar, Avoided criticality in near-optimally doped high-temperature superconductors, *Phys. Rev. B* **76**, 092503 (2007).
- [14] M. Civelli, Doping-driven evolution of the superconducting state from a doped Mott insulator: Cluster dynamical mean-field theory, *Phys. Rev. B* **79**, 195113 (2009).

- [15] M. Civelli, M. Capone, A. Georges, K. Haule, O. Parcollet, T. D. Stanescu, and G. Kotliar, Nodal-Antinodal Dichotomy and the Two Gaps of A Superconducting Doped Mott Insulator, *Phys. Rev. Lett.* **100**, 046402 (2008).
- [16] A. Macridin, M. Jarrell, Th. Maier, and G. A. Sawatzky, Physics of cuprates with the two-band Hubbard model: The validity of the one-band Hubbard model, *Phys. Rev. B* **71**, 134527 (2005).
- [17] S. S. Kancharla, B. Kyung, D. Sénéchal, M. Civelli, M. Capone, G. Kotliar, and A.-M. S. Tremblay, Anomalous superconductivity and its competition with antiferromagnetism in doped Mott insulators, *Phys. Rev. B* **77**, 184516 (2008).
- [18] P. Corboz, S. R. White, G. Vidal, and M. Troyer, Stripes in the two-dimensional t - J model with infinite projected entangled-pair states, *Phys. Rev. B* **84**, 041108(R) (2011).
- [19] M. Aichhorn, E. Arrigoni, M. Potthoff, and W. Hanke, Variational cluster approach to the Hubbard model: Phase-separation tendency and finite-size effects, *Phys. Rev. B* **74**, 235117 (2006).
- [20] D. J. Scalapino, A common thread: The pairing interaction for unconventional superconductors, *Rev. Mod. Phys.* **84**, 1383 (2012).
- [21] M. Balzer, W. Hanke, and M. Potthoff, Importance of local correlations for the order parameter of high- T_c superconductors, *Phys. Rev. B* **81**, 144516 (2010).
- [22] N. Gauquelin, D. G. Hawthorn, G. A. Sawatzky, R. X. Liang, D. A. Bonn, W. N. Hardy, and G. A. Botton, Atomic scale real-space mapping of holes in $\text{YBa}_2\text{Cu}_3\text{O}_{6+\delta}$, *Nat. Commun.* **5**, 4275 (2014).
- [23] V. J. Emery, Theory of High- T_c Superconductivity in Oxides, *Phys. Rev. Lett.* **58**, 2794 (1987).
- [24] C. M. Varma, S. Schmitt-Rink, and E. Abrahams, Charge transfer excitations and superconductivity in ionic metals, *Solid State Commun.* **62**, 681 (1987).
- [25] O. K. Andersen, A. I. Liechtenstein, O. Jepsen, and F. Paulsen, LDA energy bands, low-energy Hamiltonians, t' , t'' , $t_{\perp}(k)$, and J_{\perp} , *J. Phys. Chem. Solids* **56**, 1573 (1995).
- [26] L. Fratino, P. Sémon, G. Sordi, and A.-M. S. Tremblay, Pseudogap and superconductivity in two-dimensional doped charge-transfer insulators, *Phys. Rev. B* **93**, 245147 (2016).
- [27] J. Zaanen, G. A. Sawatzky, and J. W. Allen, Band Gaps and Electronic Structure of Transition-Metal Compounds, *Phys. Rev. Lett.* **55**, 418 (1985).
- [28] C. Weber, C. Yee, K. Haule, and G. Kotliar, Scaling of the transition temperature of hole-doped cuprate superconductors with the charge-transfer energy, *Europhys. Lett.* **100**, 37001 (2012).
- [29] D. Sénéchal, Bath optimization in the cellular dynamical mean field theory, *Phys. Rev. B* **81**, 235125 (2010).
- [30] D. Sénéchal, Cluster dynamical mean field theory, in *Strongly Correlated Systems* (Springer, Berlin, 2012), pp. 341–371.
- [31] E. Pavarini, E. Koch, and P. Coleman, 13 quantum cluster methods: CPT and CDMFT, Autumn School organized by the Forschungszentrum Jülich and the German Research School for Simulation Sciences at Forschungszentrum Jülich.
- [32] A. Foley, S. Verret, A.-M. S. Tremblay, and D. Senéchal, Coexistence of superconductivity and antiferromagnetism in the Hubbard model for cuprates, *Phys. Rev. B* **99**, 184510 (2019).
- [33] E. Koch, G. Sangiovanni, and O. Gunnarsson, Sum rules and bath parametrization for quantum cluster theories, *Phys. Rev. B* **78**, 115102 (2008).
- [34] Th. Maier, M. Jarrell, Th. Pruschke, and J. Keller, d -Wave Superconductivity in the Hubbard Model, *Phys. Rev. Lett.* **85**, 1524 (2000).
- [35] B. O. Wells, Z. X. Shen, D. S. Dessau, W. E. Spicer, D. B. Mitzi, L. Lombardo, A. Kapitulnik, and A. J. Arko, Evidence for k -dependent, in-plane anisotropy of the superconducting gap in $\text{Bi}_2\text{Sr}_2\text{CaCu}_2\text{O}_{8+\delta}$, *Phys. Rev. B* **46**, 11830 (1992).
- [36] W. N. Hardy, D. A. Bonn, D. C. Morgan, R. Liang, and K. Zhang, Precision Measurements of the Temperature Dependence of λ in $\text{YBa}_2\text{Cu}_3\text{O}_{6.95}$: Strong Evidence for Nodes in the Gap Function, *Phys. Rev. Lett.* **70**, 3999 (1993).
- [37] H. Ding, T. Yokoya, J. C. Campuzano, T. Takahashi, M. Randeria, M. R. Norman, T. Mochiku, K. Kadowaki, and J. Giapintzakis, Spectroscopic evidence for a pseudogap in the normal state of underdoped high- T_c superconductors, *Nature (London)* **382**, 51 (1996).
- [38] M. R. Norman, D. Pines, and C. Kallin, The pseudogap: Friend or foe of high T_c ? *Adv. Phys.* **54**, 715 (2005).
- [39] C. Collignon, S. Badoux, S. A. A. Afshar, B. Michon, F. Laliberté, O. Cyr-Choinière, J.-S. Zhou, S. Licciardello, S. Wiedmann, N. Doiron-Leyraud *et al.*, Fermi-surface transformation across the pseudogap critical point of the cuprate superconductor $\text{La}_{1.6-x}\text{Nd}_{0.4}\text{Sr}_x\text{CuO}_4$, *Phys. Rev. B* **95**, 224517 (2017).
- [40] A. G. Loeser, Z.-X. Shen, D. S. Dessau, D. S. Marshall, C. H. Park, P. Fournier, and A. Kapitulnik, Excitation gap in the normal state of underdoped $\text{Bi}_2\text{Sr}_2\text{CaCu}_2\text{O}_{8+\delta}$, *Science* **273**, 325 (1996).
- [41] B. Kyung, S. S. Kancharla, D. Sénéchal, A.-M. S. Tremblay, M. Civelli, and G. Kotliar, Pseudogap induced by short-range spin correlations in a doped Mott insulator, *Phys. Rev. B* **73**, 165114 (2006).
- [42] S. Sakai, M. Civelli, and M. Imada, Hidden Fermionic Excitation Boosting High-Temperature Superconductivity in Cuprates, *Phys. Rev. Lett.* **116**, 057003 (2016).
- [43] T. D. Stanescu and G. Kotliar, Fermi arcs and hidden zeros of the Green function in the pseudogap state, *Phys. Rev. B* **74**, 125110 (2006).
- [44] G. Sordi, K. Haule, and A.-M. S. Tremblay, Finite Doping Signatures of the Mott Transition in the Two-Dimensional Hubbard Model, *Phys. Rev. Lett.* **104**, 226402 (2010).
- [45] T. D. Stanescu and P. Phillips, Pseudogap in Doped Mott Insulators is the Near-Neighbor Analog of the Mott Gap, *Phys. Rev. Lett.* **91**, 017002 (2003).
- [46] H. Yokoyama, M. Ogata, Y. Tanaka, K. Kobayashi, and H. Tsuchiura, Crossover between BCS superconductor and doped Mott insulator of d -wave pairing state in two-dimensional Hubbard model, *J. Phys. Soc. Jpn.* **82**, 014707 (2012).
- [47] L. Fratino, P. Sémon, G. Sordi, and A.-M. S. Tremblay, An organizing principle for two-dimensional strongly correlated superconductivity, *Sci. Rep.* **6**, 22715 (2016).
- [48] G. Sordi, K. Haule, and A.-M. S. Tremblay, Mott physics and first-order transition between two metals in the normal-state phase diagram of the two-dimensional Hubbard model, *Phys. Rev. B* **84**, 075161 (2011).
- [49] D. Sénéchal, D. Perez, and M. Pioro-Ladriere, Spectral Weight of the Hubbard Model Through Cluster Perturbation Theory, *Phys. Rev. Lett.* **84**, 522 (2000).
- [50] J. L. Tallon, C. Bernhard, H. Shaked, R. L. Hitterman, and J. D. Jorgensen, Generic superconducting phase behavior in High- T_c

- cuprates: T_c variation with hole concentration in $\text{YBa}_2\text{Cu}_3\text{O}_{7-\delta}$, [Phys. Rev. B **51**, 12911 \(1995\)](#).
- [51] Y. He, M. Hashimoto, D. Song, S.-D. Chen, J. He, I. M. Vishik, B. Moritz, D.-H. Lee, N. Nagaosa, J. Zaanen *et al.*, Rapid change of superconductivity and electron-phonon coupling through critical doping in Bi-2212, [Science **362**, 62 \(2018\)](#).
- [52] A. Liebsch and H. Ishida, Temperature and bath size in exact diagonalization dynamical mean field theory, [J. Phys.: Condens. Matter **24**, 053201 \(2011\)](#).
- [53] A. V. Mallik, G. K. Gupta, V. B. Shenoy, and H. R. Krishnamurthy, Surprises in the t - J model: Implications for cuprates, [arXiv:1805.02429](#).